ACCSCIENCE PUBLISHING

International Journal of Bioprinting

RESEARCH ARTICLE

Development and assessment of dimethyl sulfoxide-free antifreeze gelatin methacryloyl hydrogels for integrated three-dimensional bioprinting and cryopreservation

Supplementary File

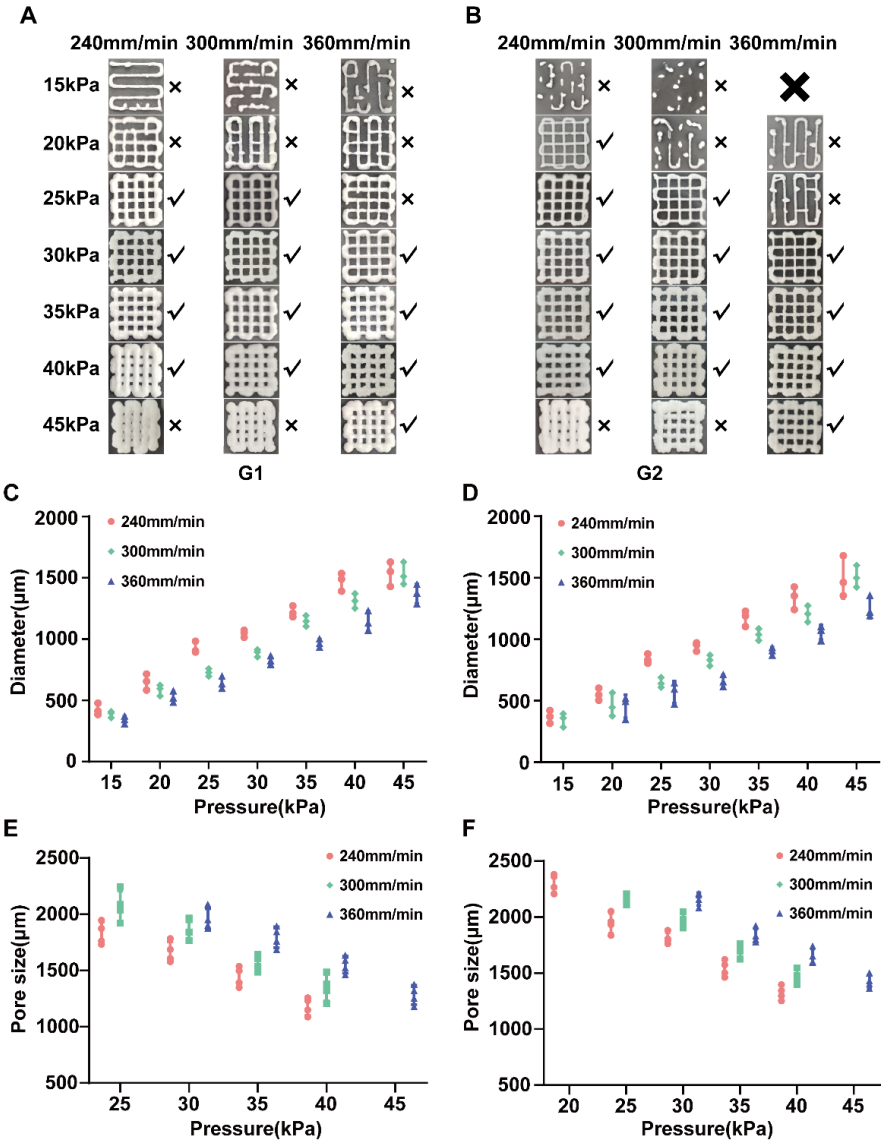

Figure S1. Effects of extrusion pressure, nozzle size, and printing speed on scaffold fidelity and structural dimensions of gelatin methacryloyl-based hydrogels with different concentrations. (A, B) Representative images of printed scaffolds fabricated from the G1 and G2 groups under varying printing conditions. (C, D) Quantitative analysis of scaffold filament diameter for G1 and G2, respectively. (E, F) Quantitative analysis of pore size for G1 and G2, respectively. Data are presented as mean ± standard deviation (diameter: $n = 3$ independent prints per condition; pore size: $n = 4$ independent prints per condition).

Note: √ indicates success and × indicates failure.

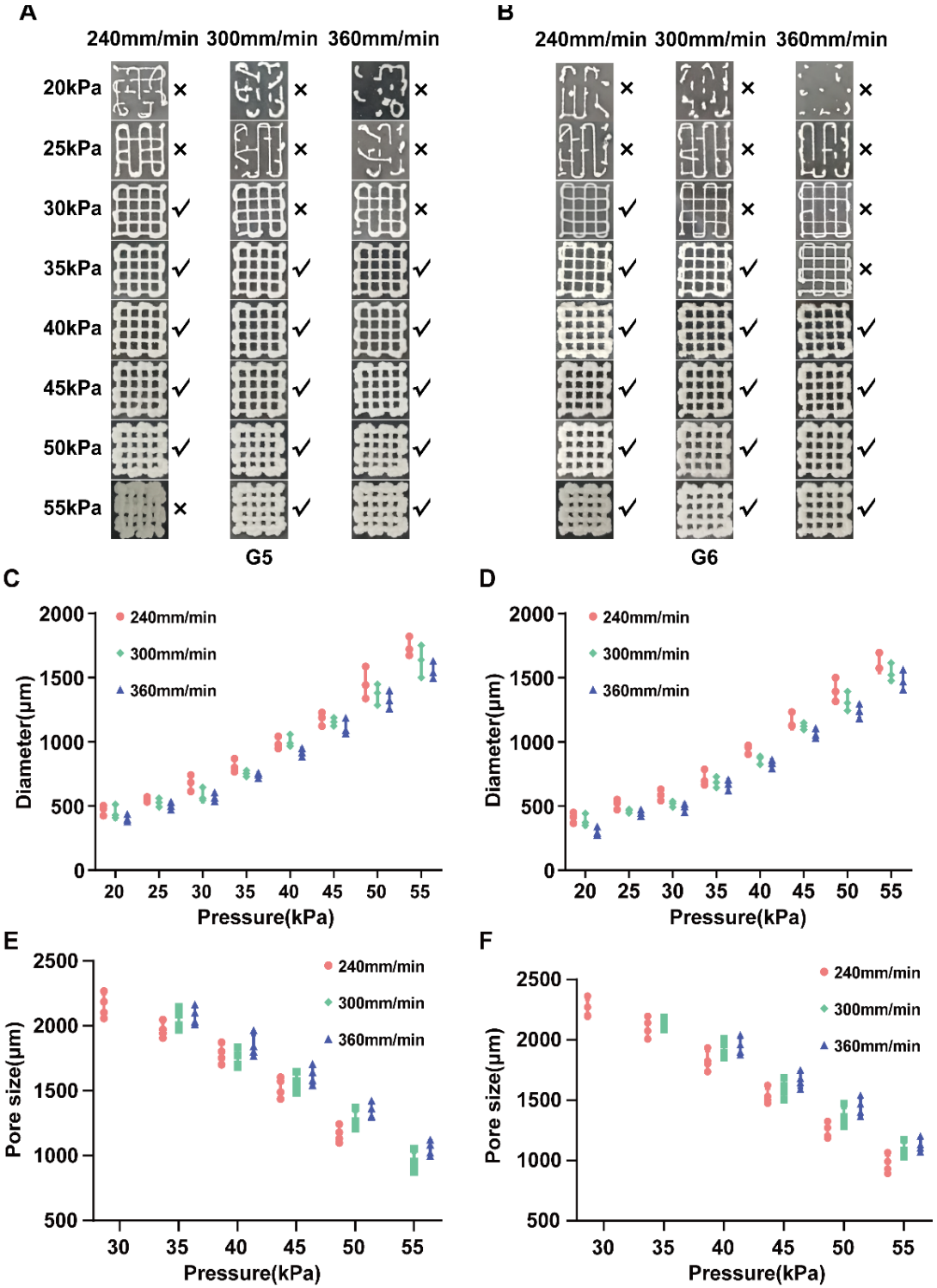

Figure S2. Effects of extrusion pressure, nozzle size, and printing speed on scaffold fidelity and structural dimensions of gelatin methacryloyl-based hydrogels with different concentrations. (A, B) Representative images of printed scaffolds fabricated from the G5 and G6 groups under varying printing conditions. (C, D) Quantitative analysis of scaffold filament diameter for G5 and G6, respectively. (E, F) Quantitative analysis of pore size for G5 and G6, respectively. Data are presented as mean ± standard deviation (diameter: $n = 3$ independent prints per condition; pore size: $n = 4$ independent prints per condition).

Note: √ indicates success and × indicates failure.

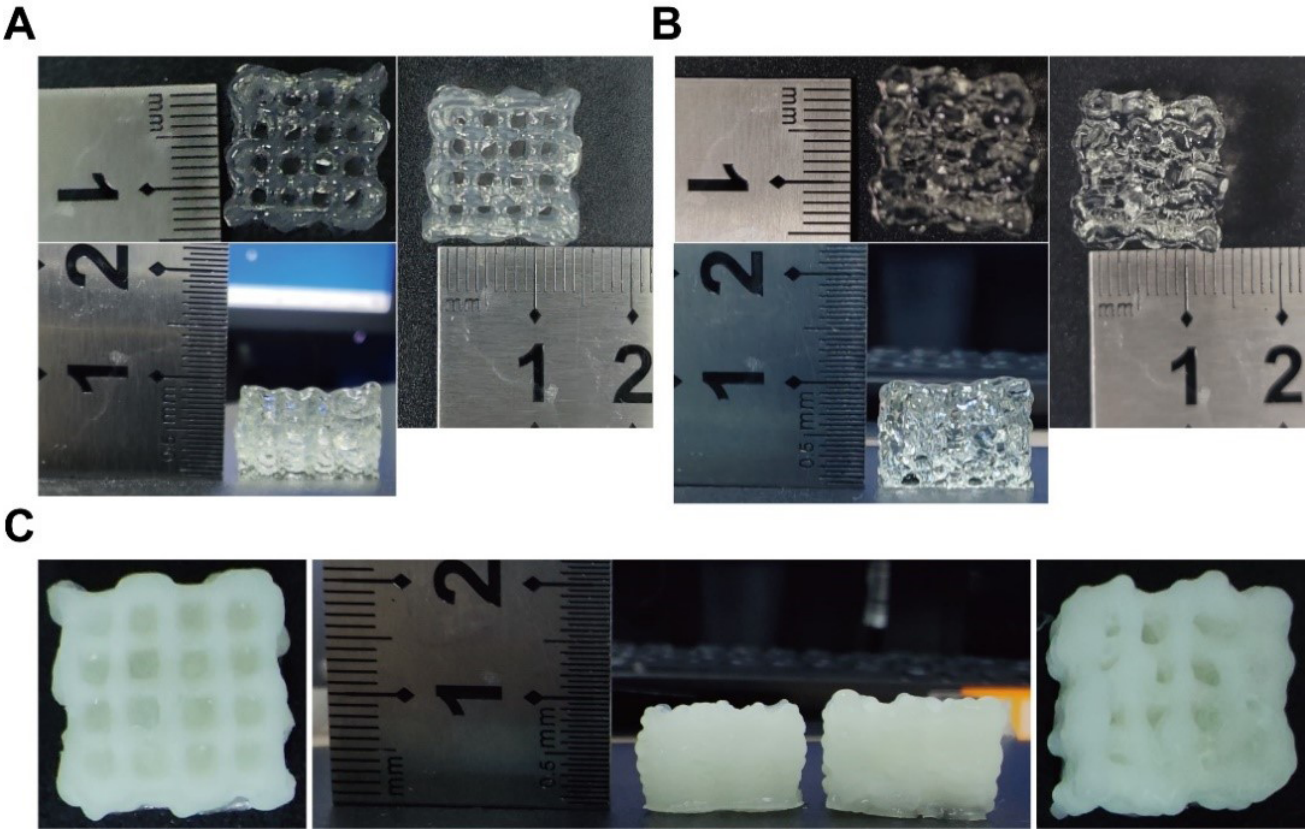

Figure S3. Validation of the maximum printable height for 900 μm diameter scaffolds. (A) Top and side views of scaffolds printed at a height of 9 mm. (B) Top and side views of scaffolds printed at a height of 9.9 mm. (C) Comparison structural integrity of the 9 mm and 9.9 mm scaffolds after freezing in −196 °C.

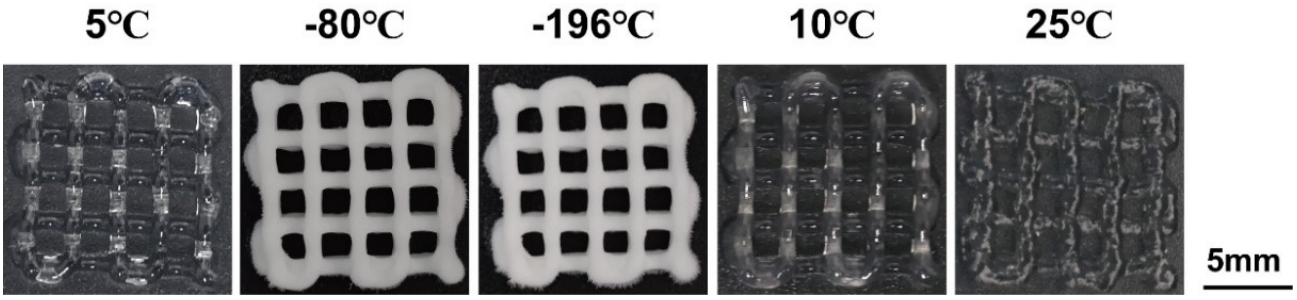

Figure S4. Morphological comparison of ultraviolet-cured, four-layer scaffolds (900 μm diameter) before and after cryopreservation. Scale bar: 5 mm.

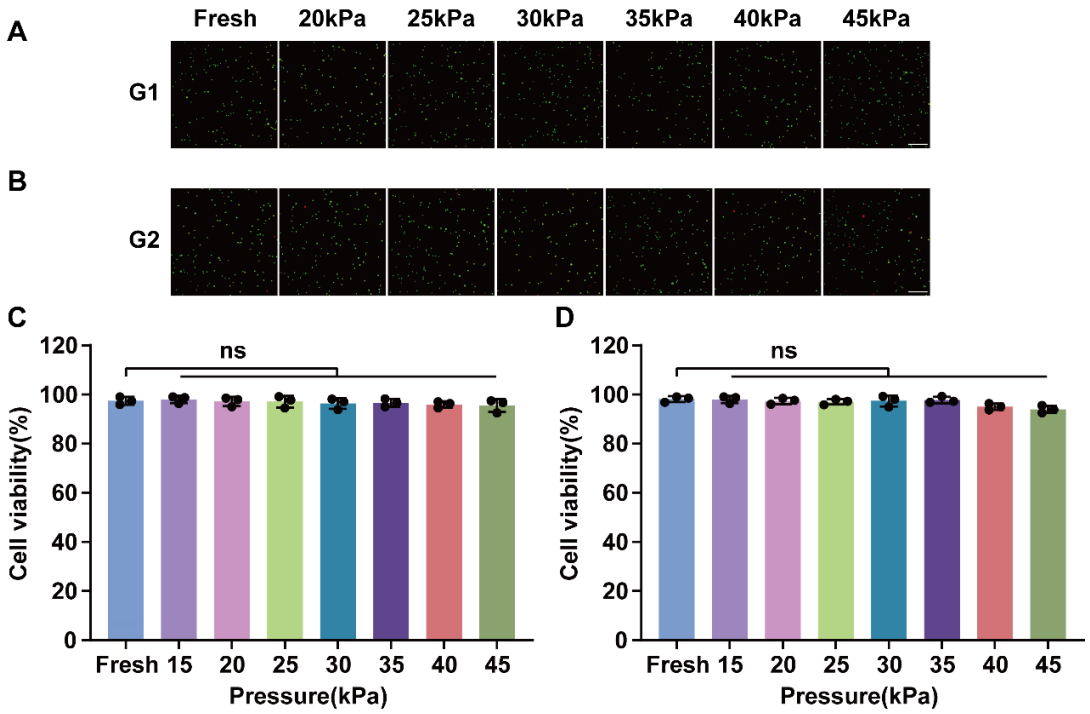

Figure S5. Cell viability of 3T3 fibroblasts under different printing conditions. (A, B) Representative live/dead fluorescence images of constructs printed with the G1 and G2 groups, respectively. Scale bar: 100 μm; magnification: 20×. (C, D) Quantitative analysis of cell viability for G1 and G2 under varying printing conditions. Data are presented as mean ± standard deviation (n = 3 independent experiments for each condition, ns: not significant).

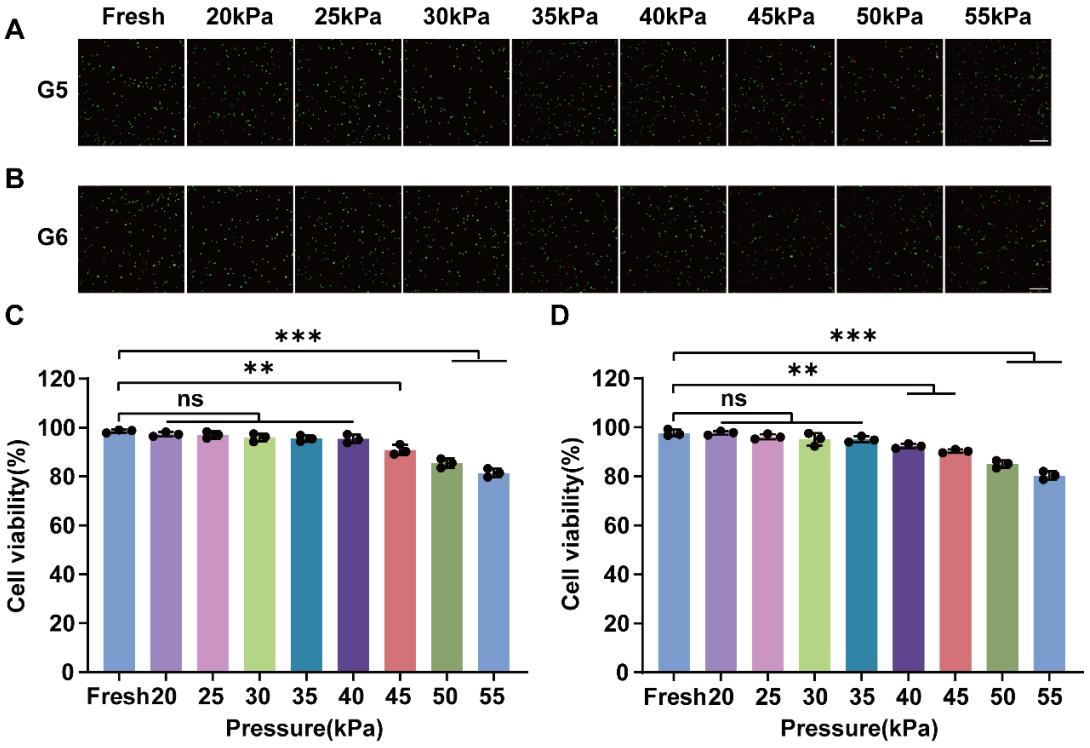

Figure S6. Cell viability of 3T3 fibroblasts under different printing conditions. (A, B) Representative live/dead fluorescence images of constructs printed with the G5 and G6 groups, respectively. Scale bar: 100 μm; magnification: 20×. (C, D) Quantitative analysis of cell viability for G5 and G6 under varying printing conditions. Data are presented as mean ± standard deviation (n=3 independent experiments for each condition; $^{**}p < 0.01$, $^{***}p < 0.001$, ns: not significant).

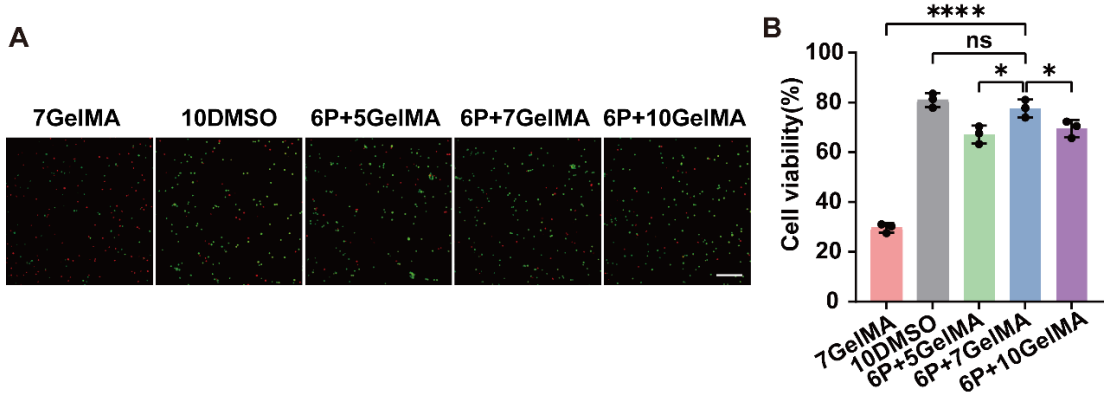

Figure S7. Cryopreservation performance of 3T3 fibroblasts using different antifreeze hydrogel formulations. (A) Representative live/dead fluorescence images of 3T3 cells following cryopreservation in the indicated hydrogel groups. Scale bar: 100 μm; magnification: 20×. (B) Quantitative analysis of post-thaw cell viability. Data are presented as mean ± standard deviation (n=3 independent cryopreservation experiments per condition; *p < 0.05, ****p < 0.0001, ns: not significant).
Abbreviations: DMSO: Dimethyl sulfoxide; GelMA: Gelatin methacryloyl; P: L-proline.

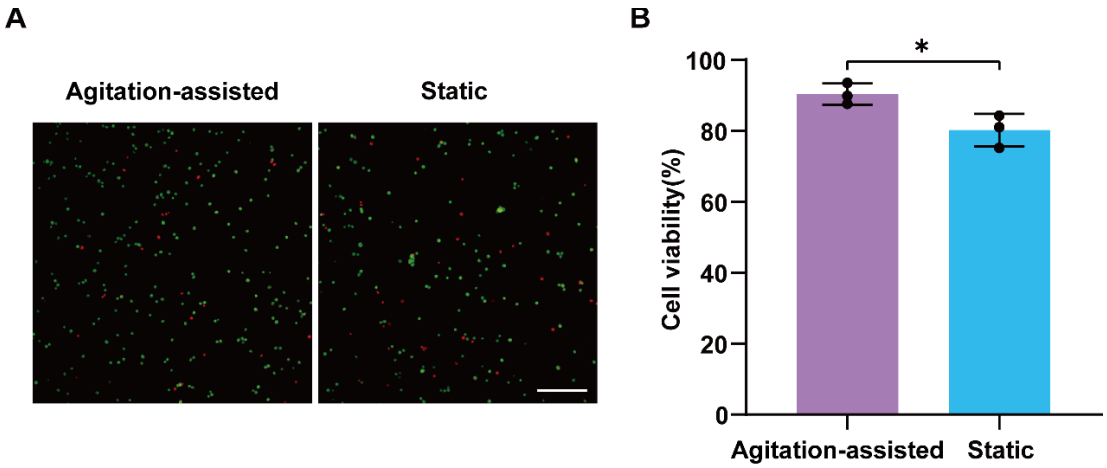

Figure S8. Optimization of the enzymatic digestion protocol for enhanced cell recovery. (A) Representative live/dead staining images of cells recovered via agitation-assisted and static methods. Scale bar: 100 μm; magnification: 20×. (B) Comparison of cell viability between the two digestion groups. Data are presented as mean ± standard deviation (n = 3 independent experiments for each condition; *p < 0.05).

Table S1. Thermal properties of materials used in the COMSOL finite element model

Parameter	Symbol	Value (Unit)	Source
Density	ρ	1,000 kg/m^3	1
Thermal conductivity	k	0.57 W/(m^2·K)	1
Specific heat	C_p	4.136 kJ/(kg · K)	1
Ratio of specific heats	γ	1.33	1

Table S2. Detailed experimental parameters and cooling/warming rates for hydrogel scaffold cryopreservation

	Step	Temp (℃)	Time (min)	Step	Temp (℃)	Cooling rate (℃/min)	Sample volume	Container	Thawing	Warming rate (℃/min)
F-1	Equilibrium	25 to 4	30	Programmed cooling	4 to −80	0.82 ± 0.34	2-layer scaffold	2 mL cryovial	37 ℃ water bath	133.17 ± 1.35
F-2	Equilibrium	25 to 4	10	−80 ℃ freezer	4 to −80	5.38 ± 0.77	2-layer scaffold	2 mL cryovial	37 ℃ water bath	130.32 ± 1.19
F-3	Equilibrium	25 to 4	10	Liquid nitrogen	4 to −196	63.27 ± 2.05	2-layer scaffold	2 mL cryovial	37 ℃ water bath	135.66 ± 1.72
F-1’	Equilibrium	25 to 4	30	Programmed cooling	4 to −80	1.26 ± 0.28	2-layer scaffold	None	37 ℃ water bath	131.81 ± 1.87
F-2’	Equilibrium	25 to 4	10	−80 ℃ freezer	4 to −80	8.68 ± 0.62	2-layer scaffold	None	37 ℃ water bath	132.47 ± 1.04
F-3’	Equilibrium	25 to 4	10	Liquid nitrogen	4 to −196	227.34 ± 1.53	2-layer scaffold	None	37 ℃ water bath	132.58 ± 1.63

References

1. Ravanbakhsh H, Luo Z, Zhang X, et al. Freeform Cell-Laden Cryobioprinting for Shelf-Ready Tissue Fabrication and Storage. *Matter.* 2022;5(2):573-593.

doi:10.1016/j.matt.2021.11.020